Int. J. Electrochem. Sci., 16 **(2021)** Article ID: 210735, doi: 10.20964/2021.07.65

International Journal of
ELECTROCHEMICAL
SCIENCE
www.electrochemsci.org

Conversion of Methane to Methanol using WO_3/TiO_2 Porous Photocatalyst

*Marcos Yovanovich, Araceli Jardim da Silva, Rodrigo F. B. de Souza, Valter Ussui†, Almir Oliveira Neto, Dolores R. R. Lazar**

Instituto Pesquisas Energéticas e Nucleares - IPEN/CNEN-SP, Av. Prof. Lineu Prestes, 2242, Cidade Universitária, 05508-000, São Paulo, SP, Brazil
*E-mail: drlazar@ipen.br
† Note: This paper is dedicated to the memory of Prof. Valter Ussui who passed away on January 21, 2021.

Received: 14 March 2021 / *Accepted:* 8 May 2021 / *Published:* 31 May 2021

The conversion of methane into methanol is one of the great challenges in the photocatalysis. In this investigation WO_3/TiO_2 photocatalysts was synthesized by sodium borohydride ($NaBH_4$) method. The tungsten concentration was studied in the range of 5 to 20 atomic ratio. XRD results revealed a TiO_2 anatase phase and WO_3 peaks near the background noise. However, WO_3 presence has been highlighted by Raman spectroscopy, indicating the existence of both orthorhombic and amorphous phase. The photocatalyst experiments showed that all materials enable the methanol production in UVC irradiation, and only the materials with WO_3 content produced the alcohol in white light irradiation. The high conversion was observed for $WO_{3(10)}/TiO_{2(90)}$ with 3.5 mmol h^{-1}. The conversion of methane to methanol was most promising using $WO_{3(10)}/TiO_{2(90)}$ due high conversion and no other products observed in FTIR spectra.

Keywords: methane into methanol, WO_3/TiO_2 photocatalysts, photo-reactor.

1. INTRODUCTION

Methane is the main component of natural gas, therefore it is a promising source of primary energy, due to its large global reserves that rival those of petroleum [1]. However, in the atmosphere it is also a powerful greenhouse gas, which effects are up to thirty times greater than CO_2. In order to overcome this drawback, this hydrocarbon can be transformed to liquid fuels and commodity chemicals, either directly or indirectly, gaining in the environmental and financial areas, because these products have a higher market value than gas [2].

The conversion of methane into some more versatile product is usually carried out by means of Fischer-Tropsch synthesis [3, 4]. Meanwhile, this process requires a large amount of energy to generate steam and the separation products is needed, incurring a high cost and energy penalty [2]. The challenge to find catalytic processes that allow mild conditions is due to CH_4 stability and its low polarization that make it hard to break the C-H bond [3, 5-8].

Photocatalysis has been a promising method for many applications such as: elimination of organic pollutants in water and in the atmosphere [9], transformation of organic compounds [10, 11] and others advanced oxidation process for environmental or conversion reactions. Studies for the photocatalytic conversion of methane into methanol have recently been performed [11-14]. On the surface of an irradiated catalyst there is charge separation, which activates water and generates the hydroxyl radical that makes radical substitution in methane (eq 1-3).

$$\text{Semiconductor} + hv \rightarrow e^- + h^+ \quad (1)$$

$$h^+ + H_2O_{ads} \rightarrow HO\bullet_{ads} + H^+ \quad (2)$$

$$CH_4 + HO\bullet_{ads} \rightarrow CH_3OH + H\bullet \quad (3)$$

Tian et al. [15] reviewed the research progress concerning methane to methanol photocatalytic conversion. It was pointed out that it is a complex process affected by photocatalyst chemical and physical characteristics and reaction conditions (temperature, time, presence of oxidant and sacrificial agents, catalysts dispersion, light source and experimental apparatus). As a consequence, the selectivity and methanol yield fluctuate a lot and the comparison becomes difficult, even for catalysts with the same composition.

In the last twenty years, the number of publications about methane to methanol photocatalytic conversion increased, especially regarding the use of WO_3 catalyst, due to its chemical stability, non-toxicity and bandgap (2.7 eV) which allows a visible light absorption. However, most of studies employing WO_3 for methane to methanol conversion were performed under ultraviolet light in heated systems (55-94 ^oC). Doping WO_3 structure has been evaluated to enhance photocatalytic activation. The reaction performed with mesoporous La^{3+} doped WO_3, in a batch reactor under UVC visible light and 55 ^oC, enables methanol production two times higher compared to undoped WO_3 [11, 15]. The addition of Fe^{3+} in WO_3 structure allows an increase of methanol production by a factor of 2.5 under ambient conditions [13, 15]

TiO_2 has been studied for methane to methanol conversion since 2004. The advantages of this catalyst include its chemical stability, non-toxicity and low cost. Due to its large bandgap (3.2 eV) this reaction is always performed under ultraviolet light and, in order to allow the reaction under solar light, modification of TiO_2 structure is recommended. As an example, iron-decorated TiO_2 enhances four times methanol production, compared to pure TiO_2 [15].

WO_3/TiO_2 heterostructured materials have been investigated for some photocatalytic processes due to the WO_3 suitable conduction band edge to form a type II hetero-junction with TiO_2. This configuration enables the transfer of photo-generated electrons from TiO_2 to WO_3 [9, 16]. In addition, the WO_3/TiO_2 heterostructures present activity at wavelengths greater than for the ultraviolet light [16]. Research groups reported differences in hetero-material activities based on tungsten and titanium

oxides, and these differences are associated with the particle size, content, and crystal phase of WO_3 which influence the charge separation efficacy at TiO_2/WO_3 interface [9, 16, 17].

The configuration of reactors plays an important role in photocatalysis. Usually, the batch reactor is applied to the evaluation of photocatalyst activity due to its easy application, without the need of large amount of catalyst. However, batch reactor presents lower efficiency and difficulty in separating the products [18]. The continuous flow reactor presents more efficiency of light absorption of a catalyst that is important to increase its photocatalytic performance. Nevertheless, the short contact time between feed gas and catalyst requires a highly active photocatalyst [19]. In this work, we tested a batch reactor with a gas diffusion system through the immobilized WO_3/TiO_2 catalyst for conversion of methane into methanol. This proposed configuration combines the practicality of the batch reactor with the reduced amount of material and the elimination of sample filtration steps of the continuous flow reactor, using a catalyst thin layer and a gas diffusion system. The WO_3/TiO_2 heterostructures were produced by $NaBH_4$ reduction method.

2. MATERIALS AND METHODS

WO_3/TiO_2 catalytic systems was synthesized in different atomic compositions (5, 10, 15 and 20 atomic% of tungsten) from tungstic acid (H_2WO_4 – Aldrich) and TiO_2 (Aldrich). These powders were dispersed in a mixture of water/2-propanol 50/50 (*v/v*). Later, sodium borohydride in excess with 10 mL 0.01 mol. L^{-1} of KOH was added to the suspensions. The obtained catalysts were washed with water and dried at 70°C for 2 hours with vacuum filtered.

The catalysts were characterized by TEM using a JEOL JEM-2100 electron microscope, operated at 200 KV. The crystalline structures of materials prepared were investigated by XRD using the X-ray diffractometer model Miniflex II, with Cu kα radiation source of 0.15406 Å, where the analyses condition were set at 2θ range 20–90º, with 2 min^{-1} scan speed.

The cyclic voltammetry tests were performed using a Parstat 3000A bipotentiostat/galvanostat and a conventional three electrode cell. A Ag/AgCl (3 mol L^{-1} KCl) was used as reference electrode and Pt was used as counter electrode ($area_g$ = 2 cm^2). The working electrodes were prepared with 15 µL aliquot of each paint composed of a mixture of 8 mg of each catalyst + 750 µL of H_2O, 250 µl of isopropyl alcohol and 15 µL of 5% Nafion D-520. The experiments with catalysts prepared were performed in 1 mol L^{-1} $LiClO_4$ in acetonitrile in the potential range of -1.5V to 1.5V.

The photocatalyst experiments were performed in a PTFE photochemical reactor (1 L capacity) containing water 100 mL. This reactor was equipped with gas inlet and an adapted gas diffusion layers, where a medium-pressure mercury (254 nm, 9W) and xenon (65 W) lamp was used to provide UVC-visible and white light irradiation. The reaction temperature was maintained at 25ºC (fig 1). The methane flow passed through the carbon diffuser layer, produced with 40 mg of carbon Vulcan (Cabot ®) agglutinate with a 2% PTFE suspension (DuPont TM 30) in a mold with a radius of 12 mm and 2 mm deep and pressed for 1 hour at 80º C and 225 KgF cm^{-2}, and the porous thin layer of photocatalyst prepared by mixture 20 mg of catalyst with 2% PTFE suspension (DuPont TM 30). This set of

materials forms a paste that fill the 0.5 mm space between the carbon diffusing insert and the interface with the water.

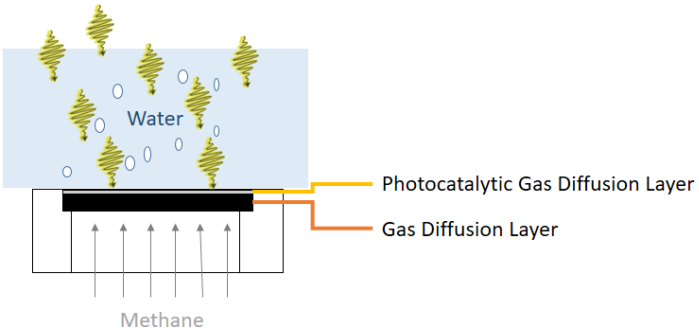

Figure 1. Schematic representation of the position of the gas diffusion thin layer with a porous photocatalytic layer in the photo-reactor for methane conversion to methanol

The quantification of methanol was obtained by Boyaci's method with Raman spectroscopy [20, 21], using Horiba Scientific MacroRam Raman spectroscopy equipment, with a 785 nm wavelength. The analytical curve was constructed in the concentration range of 0.005-1.000 mol.L^{-1} of methanol. For the following analytical curve, an intensity = 3.3509 + 3.983 [methanol] was obtained with the correlation coefficient being 0.97.

The Fourier Transform Infrared (FTIR) spectroscopy technique was used to identify the different species formed during the partial oxidation of methane in water at different times (60, 120, 300, 600, 1200, 2400 and 3600s), using a ATR-FTIR performed on an ATR accessory (MIRacle with a ZnSe Crystal Plate Pike®) installed on a Nicolet® 6700 FT-IR spectrometer equipped with a cooled MCT detector with N_2 liquid.

3. RESULTS AND DISCUSSION

The WO_3/TiO_2 photocatalysts was firstly investigated by XRD. Figure 2a shows the XRD patterns of as-synthesized photocatalysts. As can be seen, the diffraction peaks at 2θ = 25.3, 36.9, 37.6, 38.6, 48.1, 53.9, 55.1, 62.12, 62.6, 68.8, 70.3, 75.1 and 75.8 degrees correspond to the crystal planes (101), (103), (004), (112), (200), (105), (211), (213), (204), (116), (220), (215),and (301) of anatase TiO_2 (JCPDS #21-1272).

Tungsten oxides are observed, however with much lower intensity, when not convoluted with TiO_2 peaks. In figure 2b, these phases are observed with greater magnification of the diffractograms. In addition, is possible to see peaks close to noise at 2θ = 22.8, 26.3, 28.1, 27.9, 30.8, 42.1, 56.6, and 67 degrees that can be attributed to triclinic phase of WO_3 (JCPFS # 20-1323). This large difference in intensity of the TiO_2 and WO_3 peaks is probably due to the presence either in the form of highly dispersed WO_x clusters or as an amorphous layer on TiO_2 as reported in the literature [9, 17, 22-24].

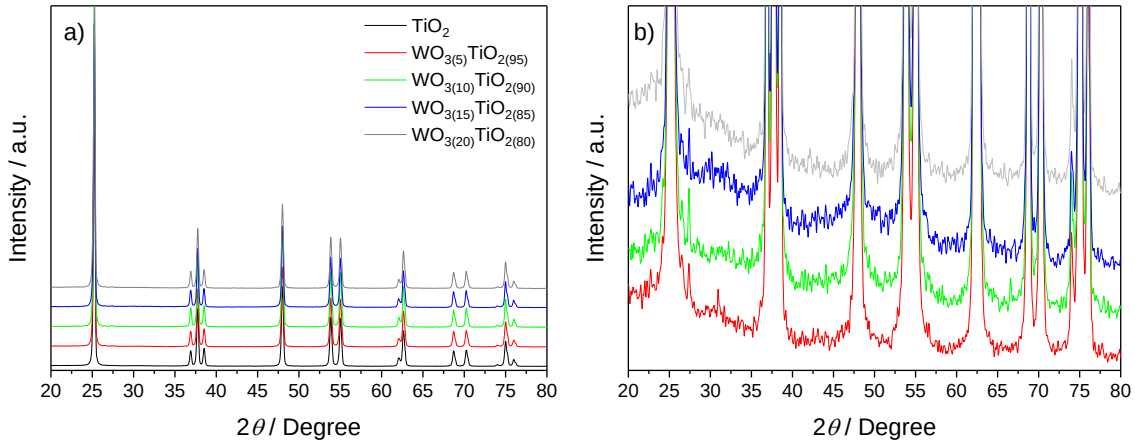

Figure 2. a) XRD pattern of W/Ti oxide based materials, b) magnification of XRD pattern (a).

Figure 3 shows the TEM of WO_3/TiO_2 materials. It can be seen that TiO_2 particle sizes are in the order of 30 to 50 nm, being very difficult to count due to particle overlay. These large structures of TiO_2 are observed for all materials, similar to reported by Song [25] and Souza [26]. Moreover, it is hard to distinguish W-based particles in these TEM images, and therefore it is difficult to estimate their particle size, as a reported by Yang [9].

The Raman spectra of WO_3/TiO_2 materials are presented in figure 4. The modes Eg, B1g, A1g, and Eg of anatase TiO_2 are clearly observed at 146 cm^{-1}, 397 cm^{-1}, 517 cm^{-1} and 638 cm^{-1} respectively [9, 27]. The characteristic Raman modes signals of the WO_3 are observed: at 278 and 317 cm^{-1} corresponding to O–W–O bending modes of bridging oxygen and at 817 cm^{-1} which is related to stretching (O-W-O) [22]. The peak at 965 cm^{-1} was reported as a marker for amorphous WO_3 [9]. The Raman spectra are in agreement with XRD patterns, indicating that WO_3 is an amorphous phase.

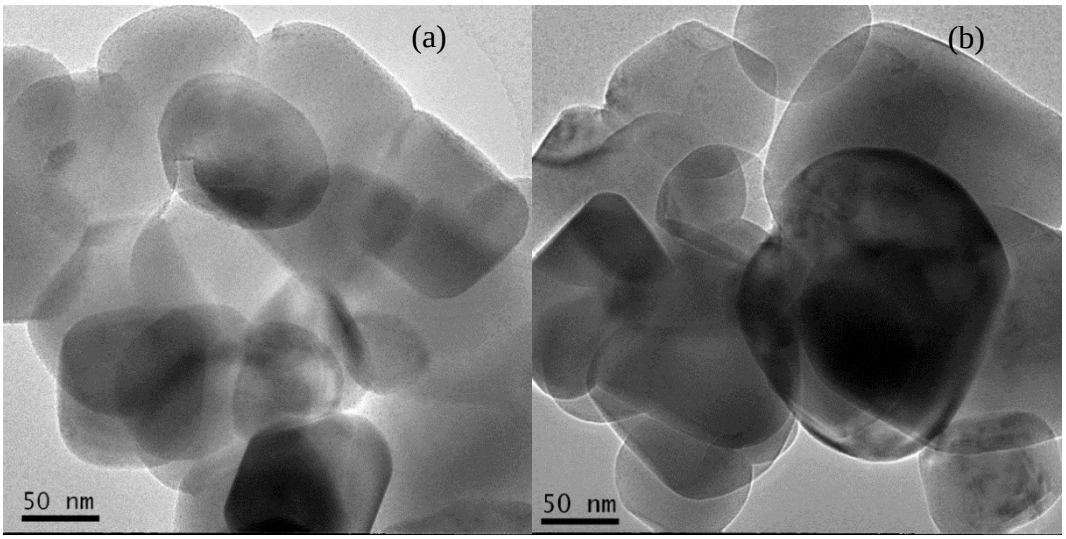

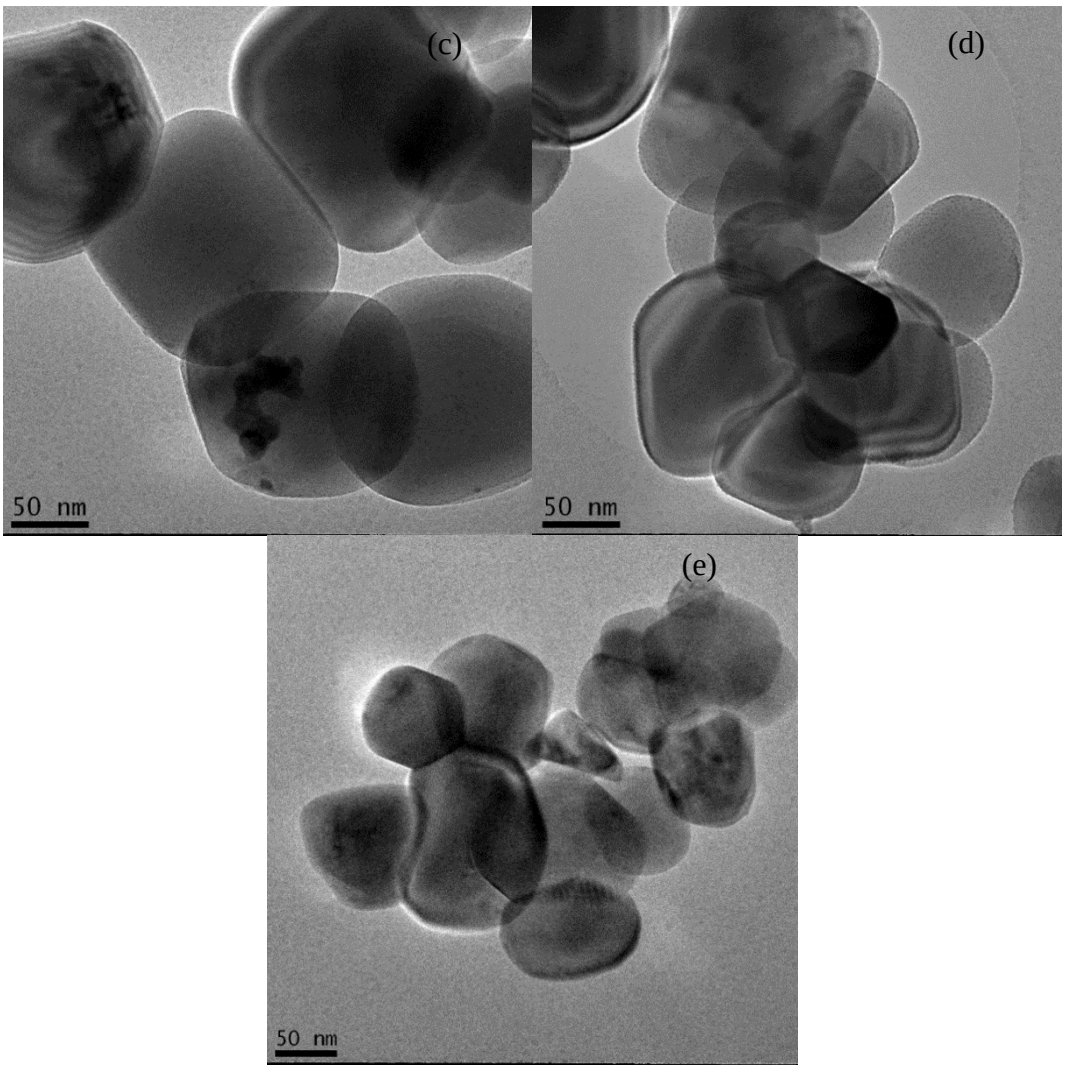

Figure 3. TEM images of studied materials: a) TiO_2, b) $WO_{3(5)}TiO_{2(95)}$, c) $WO_{3(10)}TiO_{2(90)}$, d) $WO_{3(15)}TiO_{2(85)}$, e) $WO_{3(20)}TiO_{2(80)}$

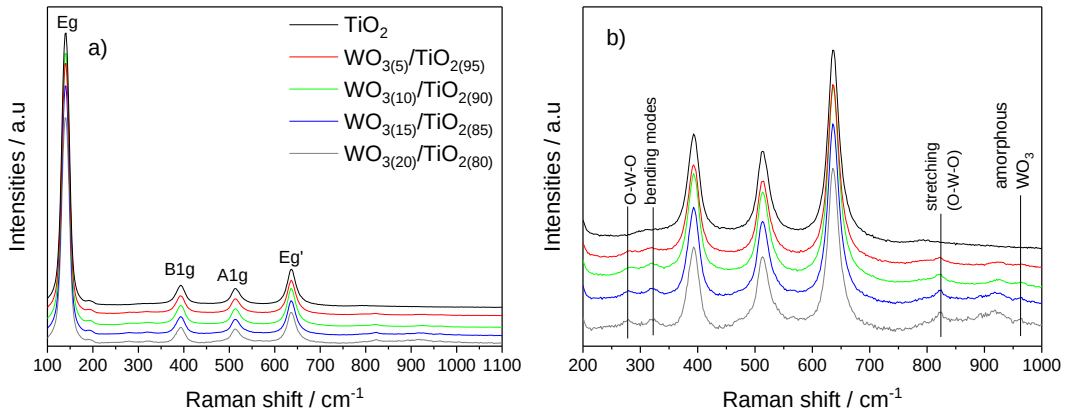

Figure 4. a) Raman spectra of WO_3/TiO_2 materials b) magnification of (a) in range of 200-1000 cm^{-1}.

Figure 5 shows the cyclic voltammograms of materials based on tungsten and titanium oxides. It is possible to observe that irreversible oxidation and reduction waves separated by ~ 2 V are reduced

with the addition of WO_3 in TiO_2. The oxidation and reduction potentials of a material could be correlated with the potentials of its HOMO and LUMO, respectively, the electrochemical bandgap seems to be lower than the optical bandgap in accordance with reference 28.

The HOMO and LUMO energy levels of WO_3/TiO_2 catalysts could be calculated from the onset oxidation potential (E^0_{Ox} (onset)) and the onset reduction potential (E^0_{Red} (onset)), as a method reported in the literature [29, 30] and represented by the equations 4-6:

$$HOMO = - [4.4\ V - E^0_{Ox}] \quad (4)$$

$$LUMO = - [4.4\ V - E^0_{red}] \quad (5)$$

$$E_g = LUMO – HOMO \quad (6)$$

The results are reported in table 1 the energy of HOMO, LUMO and Eg for WO_3/TiO_2 materials. It is possible to observe that the addition of WO_3 in TiO_2, decreases the band gap values, being in accordance with the literature results [9, 23]. Among the studied photocatalyst, the smallest bandgap is observed for the composition $WO_{3(10)}/TiO_{2(90)}$. The increase in energy of bandgap for $WO_{3(15)}/TiO_{2(85)}$ and $WO_{3(20)}/TiO_{2(80)}$ may be due to the change in the phase of WO_3 present on TiO_2 [31], based by the increase in the band in 965 cm^{-1} corresponding to the amorphous WO_3 observed in the Raman spectra (fig. 4).

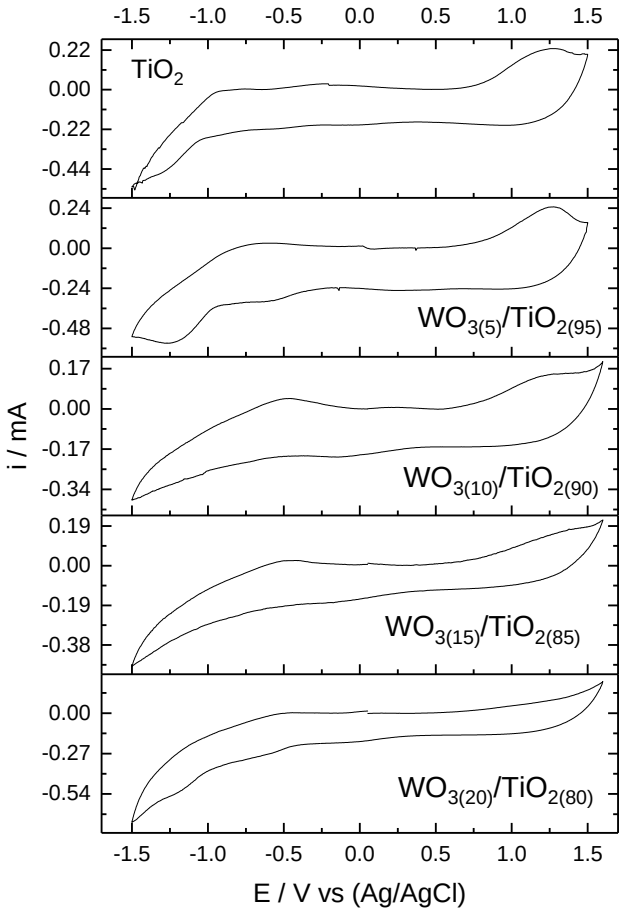

Figure 5. Cyclic voltammetry curves of WO_3/TiO_2 based electrodes. The experiments were performed in acetonitrile solution containing $LiClO_4$ 0.1 mol L^{-1}, v = 10 mV s^{-1}

Table 1. Electrochemical band gap values of TiO_2 and WO_3/TiO_2 materials calculated from HOMO and LUMO energy levels

Material	E^0_{ox} (V)	E^0_{red} (V)	HOMO (eV)	LUMO (eV)	E_g (eV)
TiO_2	0.792	-0.989	-3.612	-5.389	-1.783
$WO_{3(5)}/TiO_{2(95)}$	0.783	-0.872	-3.623	-5.272	-1.651
$WO_{3(10)}/TiO_{2(90)}$	0.709	-0.628	-3.669	-5.028	-1.341
$WO_{3(15)}/TiO_{2(85)}$	0.669	-0.719	-3.729	-5.119	-1.388
$WO_{3(20)}/TiO_{2(80)}$	0.631	-0.789	-3.771	-5.189	-1.420

The activity of these materials for methane conversion was evaluated immobilizing them in a thin porous layer on carbon diffusion gas layer where a continuous dry CH_4 flows up to the interface photocatalyst/water (fig 1). Figure 6 depicts the yield of methanol obtained after 1 h of irradiation, with UV and white light. In experiment without WO_3 photocatalyst no products formation was observed, in accordance with the literature [11]. The most active material for converting methane to methanol was $WO_{3(10)}/TiO_{2(90)}$ with both ultraviolet and white light irradiation. It is also noted that for white light the most active material has a conversion 4 times greater than with ultraviolet light. It is noted that TiO_2 does not show activity with white light.

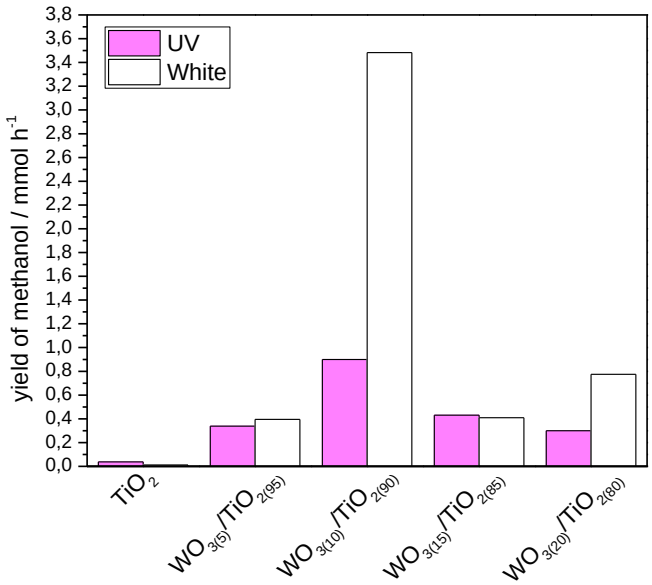

Figure 6. Yield of methanol production in the photocatalytic oxidation of CH_4 on WO_3/TiO_2, under UVC and visible light irradiation. Data corresponding to 1 h of irradiation in continuous methane flow of 50 mL min^{-1}.

As observed, when $WO_{3(10)}TiO_{2(90)}$ was at the minimum of Eg, it was at the maximum of conversion and the increase of amounts of WO_3 in the catalyst also increases the Eg and decreases activity. Yang and co-workers [9] proposed that amorphous WO_3 particles accumulate fewer electrons compared to the orthorhombic form. As the conduction band edge of amorphous WO_3 is shifted over

the one-electron reduction potential of oxygen, so just electrons injected from TiO_2 can activate the water.

During the photocatalytic experiments, an aliquot of aqueous solution was collected and analyzed by FTIR to identify the species formed. Figure 7 shows the FTIR spectra of these aliquots at time of 60 min (other times are shown in S1). It is possible to observe peaks at 1082 cm^{-1} and 1020-1030 cm^{-1} commonly attributed to methanol [20, 32]. In all materials, 1249 cm^{-1} band corresponding to CH_2 rock of formaldehyde [33] appears only for TiO_2 and $WO_{3(5)}/TiO_{2(95)}$. Another molecule reported for methane partial oxidation is the formic acid, where the 1102 cm^{-1} band, corresponding to C-O stretches [34], is present in all samples under UVC irradiation. For experiments in white light irradiation formaldehyde bands was not observed.

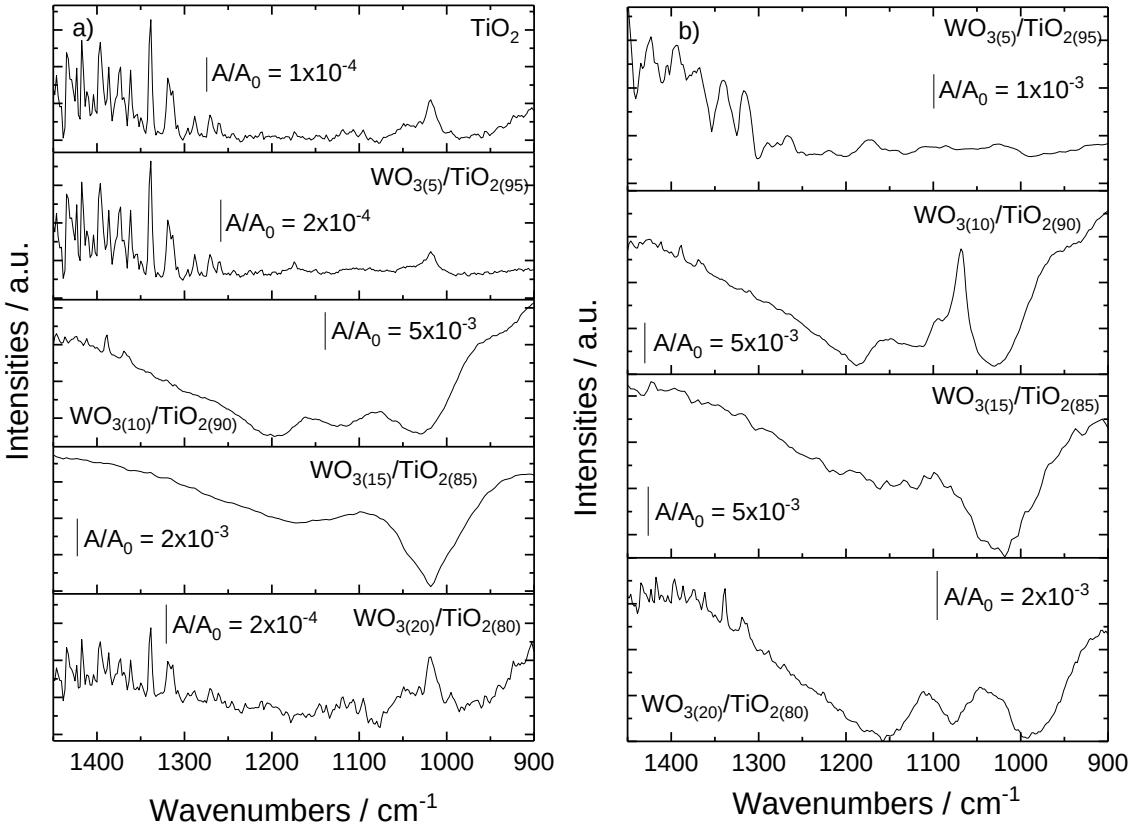

Figure 7. FTIR spectra of the aliquot taken after 60 minutes under a) UVC and b) white light.

The literature has shown that the conduction band edge of crystalline WO_3 is lower than the one-electron reduction potential of molecular oxygen [12, 35, 36], where the electrons could be accumulated in the conduction band of crystalline WO_3. This behavior reduces the amount of radicals which role in CH break. The electrons accumulated in WO_3 could react with reactive species such hydroxyl radicals generated during photocatalytic process leading the reaction to the generation of more oxidized products [12, 13]. This behavior justifies the other methane oxidation products.

4. CONCLUSION

The application of gas diffusion thin layer with the porous photocatalytic layer of WO_3/TiO_2 proved to be an efficient option for conversion of methane to methanol. The synthesis of WO_3/TiO_2 showed that almost all WO_3 deposited on TiO_2 is in an amorphous state, mainly for compositions with more than 15 atomic %. The addition of tungsten oxide in titanium oxides reduced the bandgap to a minimum for the composition $WO_{3(10)}TiO_{2(90)}$. Above that amount, WO_3 in its amorphous form caused a slight increase in E_g. WO_3-containing materials were active both under UV and white light, unlike pure TiO_2, and in white light the conversion was up to four times higher for the most active material.

ACKNOWLEDGMENTS
We are grateful to CAPES (88882.315566/2019), CNPq (302709/2020-7), FAPESP (2014/09087-4, 2014/50279-4 and 2017/11937-4), for financial supports.

SUPPLEMENTARY INFORMATION

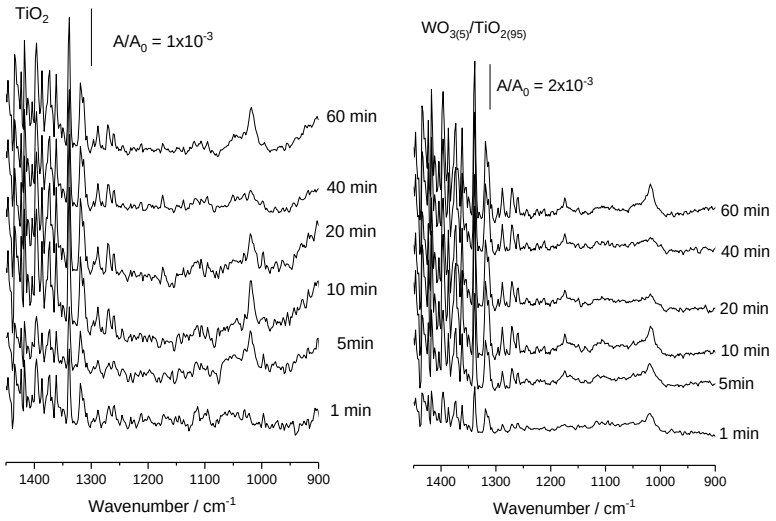

S1a: FTIR spectra taken from aliquots after different times under UVC (254 nm)

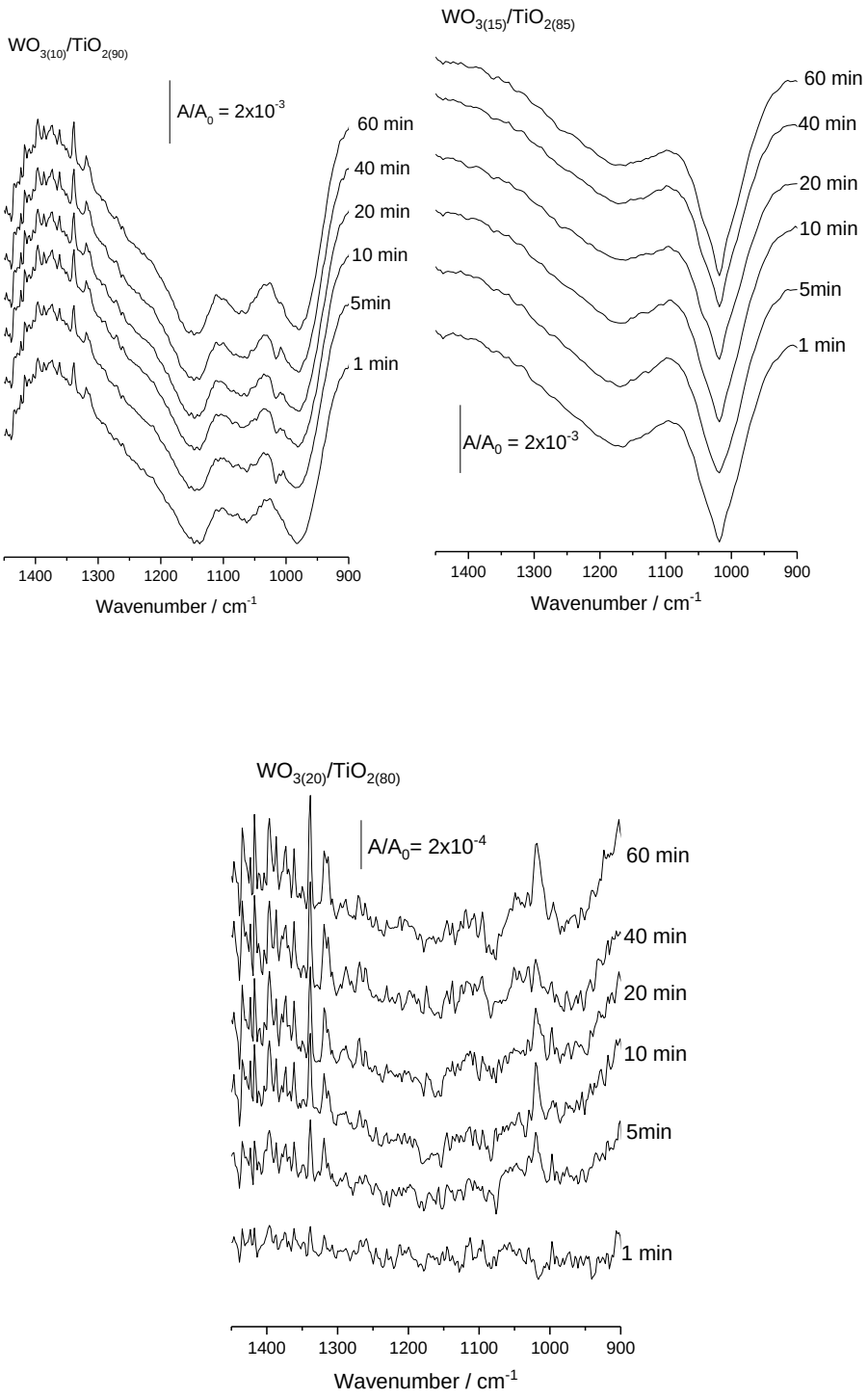

S1b FTIR spectra taken from aliquots after different times under UVC (254 nm)

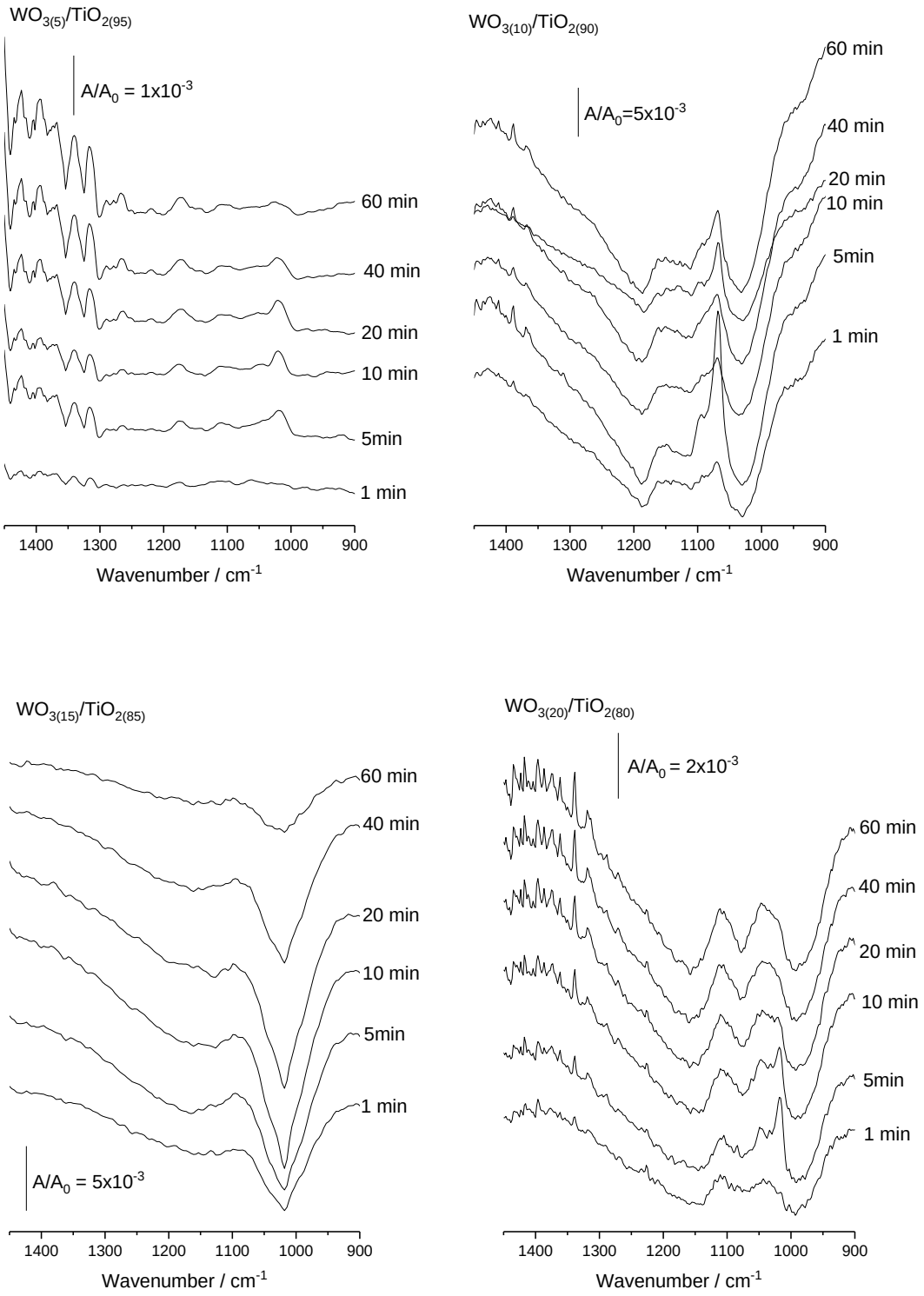

S1c: FTIR spectra taken from aliquots after different times under white light.

References

1. M.C.L. Santos, C.M. Godoi, H.S. Kang, R.F.B. de Souza, A.S. Ramos, E. Antolini, A.O. Neto, *Journal of Colloid and Interface Science*, 578 (2020) 390.
2. X. Wang, X. Du, W. Yu, J. Zhang, J. Wei, *Industrial & Engineering Chemistry Research*, 58 (2019) 10296.
3. S. Xie, S. Lin, Q. Zhang, Z. Tian, Y. Wang, *Journal of Energy Chemist*ry, 27 (2018) 1629.
4. D. Shi, J. Liu, R. Sun, S. Ji, S.M. Rogers, B.M. Connolly, N. Dimitratos, A.E.H. Wheatley, *Catalysis Today*, 316 (2018) 206.
5. D. San-José-Alonso, J. Juan-Juan, M.J. Illán-Gómez, M.C. Román-Martínez, *Applied Catalysis A: General*, 371 (2009) 54.
6. R. Shavi, V. Hiremath, J.G. Seo, *Molecular Catalysis*, 445 (2018) 232.
7. B. Lee, T. Hibino, *Journal of Catalysis*, 279 (2011) 233.
8. S.C. Nimkar, R.K. Mewada, M.A. Rosen, *International Journal of Hydrogen Energy*, 42 (2017) 28113.
9. J. Yang, X. Zhang, H. Liu, C. Wang, S. Liu, P. Sun, L. Wang, Y. Liu, *Catalysis Today*, 201 (2013) 195.
10. V. Augugliaro, M. Bellardita, V. Loddo, G. Palmisano, L. Palmisano, S. Yurdakal, *Journal of Photochemistry and Photobiology C: Photochemistry Reviews*, 13 (2012) 224.
11. K. Villa, S. Murcia-López, J.R. Morante, T. Andreu, *Applied Catalysis B: Environmental*, 187 (2016) 30.
12. K. Villa, S. Murcia-López, T. Andreu, J.R. Morante, *Applied Catalysis B: Environmental*, 163 (2015) 150.
13. J. Yang, J. Hao, J. Wei, J. Dai, Y. Li, *Fuel*, 266 (2020) 117104.
14. A. Hameed, I.M.I. Ismail, M. Aslam, M.A. Gondal, *Applied Catalysis A: General*, 470 (2014) 327.
15. Y. Tian, L. Piao, X. Chen, *Green Chemistry, Accepted april* 2021. DOI: 10.1039/D1GC00658D.
16. L.F. Paula, M. Hofer, V.P.B. Lacerda, D.W. Bahnemann, A.O.T. Patrocinio, *Photochemical & Photobiological Sciences*, 18 (2019) 2469.
17. Y. Tae Kwon, K. Yong Song, W. In Lee, G. Jin Choi, Y. Rag Do, *Journal of Catalysis*, 191 (2000) 192.
18. C. McCullagh, P.K.J. Robertson, M. Adams, P.M. Pollard, A. Mohammed, *Journal of Photochemistry and Photobiology A: Chemistry*, 211 (2010) 42.
19. J. Lang, Y. Ma, X. Wu, Y. Jiang, Y.H. Hu, *Green Chemistry*, 22 (2020) 4669.
20. M.C.L. Santos, L.C. Nunes, L.M.G. Silva, A.S. Ramos, F.C. Fonseca, R.F.B. de Souza, A.O. Neto, *ChemistrySelect*, 4 (2019) 11430.
21. I.H. Boyaci, H.E. Genis, B. Guven, U. Tamer, N. Alper, *Journal of Raman Spectroscopy*, 43 (2012) 1171.
22. K.K. Akurati, A. Vital, J.-P. Dellemann, K. Michalow, T. Graule, D. Ferri, A. Baiker, *Applied Catalysis B: Environmental*, 79 (2008) 53.
23. C. Shifu, C. Lei, G. Shen, C. Gengyu, *Powder Technology*, 160 (2005) 198.
24. S. Bai, H. Liu, J. Sun, Y. Tian, S. Chen, J. Song, R. Luo, D. Li, A. Chen, C.-C. Liu, *Applied Surface Science*, 338 (2015) 61.
25. K.Y. Song, M.K. Park, Y.T. Kwon, H.W. Lee, W.J. Chung, W.I. Lee, *Chemistry of Materials*, 13 (2001) 2349.
26. R.F.B. De Souza, G.S. Buzzo, J.C.M. Silva, E.V. Spinace, A.O. Neto, M.H.M.T. Assumpcao, *Electrocatalysis*, 5 (2014) 213.
27. H.W. Jeong, K.J. Park, D.S. Han, H. Park, *Applied Catalysis B: Environmental*, 226 (2018) 194.
28. M. Bledowski, L. Wang, A. Ramakrishnan, O.V. Khavryuchenko, V.D. Khavryuchenko, P.C. Ricci, J. Strunk, T. Cremer, C. Kolbeck, R. Beranek, *Physical Chemistry Chemical Physics*, 13 (2011) 21511.

29. Z. Han, J. Zhang, X. Yang, H. Zhu, W. Cao, *Journal of Inorganic and Organometallic Polymers and Materials,* 20 (2010) 649.
30. D. Baran, A. Balan, S. Celebi, B. Meana Esteban, H. Neugebauer, N.S. Sariciftci, L. Toppare, *Chemistry of Materials*, 22 (2010) 2978.
31. T. Tatsuma, S. Saitoh, P. Ngaotrakanwiwat, Y. Ohko, A. Fujishima*, Langmuir*, 18 (2002) 7777.
32. J. Nandenha, R.M. Piasentin, L.M.G. Silva, E.H. Fontes, A.O. Neto, R.F.B. de Souza, *Ionics*, 25 (2019) 5077.
33. K.Z. Gaca-Zając, B.R. Smith, A. Nordon, A.J. Fletcher, K. Johnston, J. Sefcik, *Vibrational Spectroscopy*, 97 (2018) 44.
34. J. Nandenha, I. Nagahama, J. Yamashita, E. Fontes, J. Ayoub, R. de Souza, F. Fonseca, A. Neto, *Int. J. Electrochem. Sci*, 14 (2019) 10819.
35. M.B. Johansson, G.A. Niklasson, L. Österlund, *Journal of Materials Research*, 27 (2012) 3130.
36. Y.M. Hunge, M.A. Mahadik, A.V. Moholkar, C.H. Bhosale, *Ultrasonics Sonochemistry*, 35 (2017) 233